Clonal stochasticity in early NK cell response to mouse cytomegalovirus is generated by mature subsets of varying proliferative ability

Darren Wethington[1,2,*], Saeed Ahmad[1], Marc Potempa[6], Giuseppe Giuliani[1,5], Oscar A. Aguilar[6], Maheshwor Poudel[1], Simon Grassmann[7], William Stewart[8], Nicholas M. Adams[7,9], Joseph C. Sun[7], Lewis L. Lanier[6,*], Jayajit Das[1,2,3,4,*]

[1]Steve and Cindy Rasmussen Institute for Genomic Medicine, Nationwide Children's Hospital, Columbus OH

[2]Biomedical Sciences Graduate Program, [3]Department of Pediatrics, [4]Pelotonia Institute for Immuno-Oncology, College of Medicine, The Ohio State University, Columbus OH

[5]Department of Physics, The Ohio State University, Columbus OH

[6]Department of Microbiology and Immunology and the Parker Institute for Cancer Immunotherapy, University of California, San Francisco CA

[7]Immunology Program, Memorial Sloan Kettering Cancer Center, New York, NY

[8]GIG Statistical Consulting, LLC, Columbus OH

[9]Department of Pathology, New York University Grossman School of Medicine, New York, NY

*Corresponding Authors, wethington.8@osu.edu, Lewis.Lanier@ucsf.edu, jayajit@gmail.com

Abstract

Natural killer (NK) cells are classically defined as innate immune cells, but experiments show that mouse cytomegalovirus (MCMV) infection in C57BL/6 mice can cause NK cells to undergo

antigen-specific proliferation and memory formation, similar to adaptive CD8+ T cells. One shared behavior between CD8+ T cells and NK cells is clonal expansion, where a single stimulated cell proliferates rapidly to form a diverse population of cells. For example, clones derived from single cells are most abundant during expansion when they are primarily CD27- for NK cells and CD62L- for T cells, phenotypes derived from precursor CD27+ and CD62L+ cells, respectively. Here we determined the mechanistic rules involving proliferation, cell death, and differentiation of endogenous and adoptively transferred NK cells in the expansion phase of the response to MCMV infection. We found that the interplay between cell proliferation and cell death of mature CD27- NK cells and a highly proliferative CD27-Ly6C- mature subtype and intrinsic stochastic fluctuations in these processes play key roles in regulating the heterogeneity and population of the NK cell subtypes. Furthermore, we estimate rates for maturation of endogenous NK cells in homeostasis and in MCMV infection and found that only NK cell growth rates, and not differentiation rates, are appreciably increased by MCMV. Taken together, these results quantify the differences between the kinetics of NK cell antigen-specific expansion from that of CD8+ T cells and unique mechanisms that give rise to the observed heterogeneity in NK cell clones generated from single NK cells in the expansion phase.

Introduction

Natural Killer (NK) cells are lymphocytes of the innate immune system and provide important protection against viral infections and tumors (Caligiuri, 2008; Vivier et al., 2008). NK cells develop in the bone marrow and express a diverse set of germline-encoded activating and inhibitory receptors (Abel et al., 2018; Biassoni, 2008; Huntington et al., 2007). Mouse

47 cytomegalovirus (MCMV) infection induces antigen-specific expansion of naïve Ly49H+ NK
48 cells in mice, followed by a contraction phase, and then the formation of long-lived adaptive NK
49 cells displaying recall responses to the same antigen (Cerwenka and Lanier, 2016; Robbins et al.,
50 2004; Schlub et al., 2011; Sun et al., 2009). The activating Ly49H receptor, encoded by *Klra8*,
51 recognizes the MCMV-encoded m157 glycoprotein and leads to activation of Ly49H+ NK cells
52 (Orr et al., 2009; Voigt et al., 2003). In humans, a similar activation of NK cells by human
53 cytomegalovirus is observed with the preferential expansion of NKG2C+ NK cells (Guma et al.,
54 2004; Hendricks et al., 2014; Ishiyama et al., 2022; Kim et al., 2019; Lopez-Verges et al., 2011).
55 The expansion, contraction, and memory formation of Ly49H+ NK cells during MCMV
56 infection bears similarity to antigen-specific responses of adaptive CD8+ T cells that generate
57 memory CD8+ T cells (Adams et al., 2020; Buchholz et al., 2013; Kaech et al., 2002; Schlub et
58 al., 2011).
59 A range of experiments investigated epigenetic changes, RNA transcription, and surface
60 protein expression in single and bulk Ly49H+ NK cells undergoing expansion and contraction in
61 mice responding to MCMV infection (Flommersfeld et al., 2021; Grassmann et al., 2019; Lau et
62 al., 2018; Martinet et al., 2015; Min-Oo et al., 2014; Nabekura et al., 2014; Potempa et al., 2022;
63 Riggan et al., 2022). These observations show that the NK cell compartment undergoes
64 phenotypic changes, resulting in changes in the abundances of varying subpopulations of cells.
65 The development of these subpopulations depends on the three main signal inputs, antigen
66 simulation of a specific receptor (e.g., Ly49H), co-stimulation, and cytokine signaling (Ni et al.,
67 2012; Peng and Tian, 2017; Romee et al., 2016). These subpopulations express distinct
68 epigenetic, transcriptomic, and protein markers imprinted by signaling and gene regulatory
69 processes. Observations of clonal expansion of barcoded single Ly49H+ NK cells adoptively

70 transferred into *Rag2*$^{-/-}$*Il2rg*$^{-/-}$ mice revealed another layer of heterogeneity where sizes and
71 compositions of NK cell clones originating from single naïve Ly49H+ NK cells vary widely
72 (Flommersfeld et al., 2021; Grassmann et al., 2019). This heterogeneity in the NK cell
73 population is regulated by the stochastic kinetics of cell proliferation, cell death, and
74 differentiation involving the subpopulations that emerge as the NK cells respond to the infection.
75 Analysis of similar heterogeneities in clonal CD8+ T cell populations have shown generation of
76 a highly proliferative short-lived effector phenotype and intrinsic stochastic fluctuations in the
77 differentiation and proliferation processes, which account for heterogeneity of the CD8+ T cell
78 clones (Buchholz et al., 2013). These effector CD8+ T cells are CD62L- and differentiate during
79 the expansion phase from upstream memory precursors that are CD62L+(Schlub et al., 2010;
80 Yang et al., 2011).

81 Despite the qualitative similarities between the antigen-specific responses of NK cells
82 and CD8+ T cells there are several marked differences. Single-cell NK clones typically undergo
83 a relatively smaller 1000× increase in number compared to the 40,000× increase in CD8+ T cell
84 populations (Adams et al., 2020). Additionally, mature CD27- NK cells grow more slowly than
85 their immature CD27+ counterparts (Buchholz et al., 2013; Hayakawa and Smyth, 2006; Paul et
86 al., 2016), whereas effector CD62L- CD8+ T cells proliferate faster than precursor CD62L+
87 subsets (Adams et al., 2020; Kretschmer et al., 2020). These data suggest there may be
88 mechanistic differences in antigen-specific NK and CD8+ T cell responses.

89 Here, we addressed whether distinct mechanisms underlie the expansion of NK cells and
90 CD8+ T cells during antigen-specific responses by performing stochastic population dynamic
91 modeling on published bulk and single-cell NK cell data collected during the expansion phase
92 following MCMV infection in C57BL/6 mice. Our analysis and modeling show that the

93 mechanistic rules that describe the expansion of CD8+ T cells are inadequate for describing the
94 development of MCMV-specific NK cells. We found that mature CD27-Ly6C- NK cells
95 undergo a greater rate of cell proliferation compared to immature CD27+ NK cells and mature
96 CD27-Ly6C+ NK cells, and mature CD27- NK cells undergo increased death relative to the
97 CD27+ immature cells. The variations in the timescales of proliferation and death processes
98 coupled with the intrinsic stochastic fluctuations within these processes among the NK cell
99 subsets regulate the heterogeneity in the sizes of the NK cell clones originated from individual
100 immature NK cells during MCMV infection. Quantification of the population kinetics of
101 Ly49H+ NK cells in MCMV infection in the expansion phase shows a 10-fold increase in the
102 cell growth rate compared to that in homeostatic conditions, whereas the effect of the infection
103 on the maturation rate appears to be negligible. We also find that growth rates of adoptive NK
104 cells in transfer experiments during MCMV infection in the expansion phase are higher than
105 those of endogenous NK cells.
106
107 **Results**
108
109 **A progressive two-state immature to mature differentiation model cannot capture the**
110 **heterogeneity of the NK cell clones in the expansion phase**
111
112 We began our investigations by studying whether a minimal two-state progressive differentiation
113 model (Fig. 1a) could describe the size and composition of NK cell clones that originated from
114 single immature Ly49H+ CD27+ NK cells at day 8 post-infection with MCMV, a time typically
115 at the peak of expansion. The differentiation of immature CD27+ to mature CD27- NK cells

116 during MCMV infection and in homeostasis has been widely documented and established in
117 previous experiments (Chiossone et al., 2009; Grassmann et al., 2019; Min-Oo et al., 2014;
118 Mitrovic et al., 2012). We used data collected by Flommersfeld *et al.(Flommersfeld et al., 2021)*,
119 in which they adoptively transferred single genetic marker barcoded Ly49H+ NK cells to a host
120 that is subsequently infected with MCMV. We characterized the NK cell clones by the means
121 and variances of the populations of CD27+ or CD27- NK cells and the co-variance between the
122 two cell types in the clones. The NK cell clones reported by Flommersfeld *et al.* contained
123 mixtures of CD27+ and CD27- NK cells. We evaluated the percentage of CD27+ NK cells in
124 each clone and computed the correlation ($C_{size\text{-}CD27+}$) of the size of the clone with the percentage
125 of CD27+ NK cells in the clones. The larger size NK cell clones contained a greater proportion
126 of the CD27- NK cells and thus produced a negative correlation between the clone size and the
127 percentage of CD27+ NK cells in individual clones (Fig. 1b). This finding is in line with that
128 found in a similar experiment by Grassmann *et al. (Grassmann et al., 2019).* These authors also
129 transferred congenically-marked CD27- and CD27+ Ly49H+ NK cells in 1:1 ratio at day 0 and
130 then assayed the expanded CD27+/- NK cells at day 8 post infection, showing a higher
131 proportion of mature CD27- NK cells compared to the immature CD27+ NK cells (Figure S2E in
132 Grassmann *et al. (Grassmann et al., 2019)*). This result is supported by other experiments
133 (Hayakawa and Smyth, 2006; Paul et al., 2016), and we used this observation to constrain our
134 model parameter space. Heterogeneity of clones of CD8+ T cells generated by antigenic
135 SIINFEKL stimulation showed a similar pattern where the largest clones in the expansion phase
136 (day 7 post-stimulation) are composed of higher fractions of the mature CD62L- CD8+ T cells
137 (Buchholz et al., 2013). Because mature CD62L- CD8+ T cells proliferate faster than the
138 immature CD62L+ CD8+ T cells (Buchholz et al., 2013; Kretschmer et al., 2020), it is intuitive

139 that a larger size of a clone can be attributed to the larger proportion of the mature CD8+ T cells
140 in the clone (Fig. 1c). In contrast, NK cells proliferate slower when they differentiate to the
141 mature CD27- phenotype. Thus, it is unclear how the similar relationship between the clone size
142 and the composition of the clones can be understood. In order to probe this question further we
143 used a stochastic model (Fig. 1a) that describes the proliferation and differentiation processes in
144 single Ly49H+ NK cells in response to MCMV infection. We do not model the MCMV infection
145 explicitly and assume that the parameters of the model capture the effects of antigen, co-receptor,
146 and cytokine stimulation and signaling and epigenetic modifications on the rates of
147 differentiation and the proliferation of the cell types. In this model, immature CD27+ NK cells
148 differentiate with a rate r to mature CD27- NK cells, and each cell type proliferates with rates, k_I
149 and k_M, respectively. The proliferation and differentiation processes are modeled as stochastic
150 events occurring with the above rates. We start our simulations with a single CD27+ NK cell and
151 evaluated the number of CD27+ and CD27- NK cells at 8 days, which represent the size and the
152 composition of a single NK cell clone. Repetitions of the stochastic simulations with the same
153 initial configuration and rates will produce clones of different sizes and compositions due to
154 intrinsic noise fluctuations in the stochastic simulations. We computed the correlation ($C_{\text{size-}}$
155 $_{\text{CD27+}}$) between the clone sizes and the percentages of the CD27+ NK cells in each clone from our
156 simulations. Our parameter scan of randomly sampled values of k_I, k_M, and r revealed that C_{size-}
157 $_{CD27+}$ is negative *only* when $k_I < k_M$ (Fig. 1d). However, the observations that CD27+ cells should
158 grow faster than CD27- cells imply $k_I > k_M$ for the NK cells. Therefore, the two-state model
159 cannot capture the heterogeneity of the NK cell clones.
160 Next, we investigated if inclusion of death of NK cells can make the model consistent
161 with the negative correlation between the clone size and the percentage of CD27+ NK cells in

each clone. We updated our proposed model to include both proliferation and death of each cell population (Fig. 1e). In such a model, each cell has a probability of proliferating according to birth rate b and probability of dying indicated by the death rate d. Cells can go through many proliferation events before undergoing death, which would indicate a positive growth rate. The net growth of the CD27+ and CD27- NK cell populations are determined by $k_I=b_I-d_I$ and $k_M=b_M-d_M$, respectively, where b_I and d_I (or b_M and d_M) are the proliferation and death rates of the immature CD27+ (or mature CD27-) NK cells. Repeating a parameter scan by randomly sampling the 5 parameters (b_I, d_I, b_M, d_M, and r) from uniform distributions and evaluating the correlation $C_{size\text{-}CD27+}$ shows that some parameter configurations can generate the negative values at the parameter values, $k_I > k_M$ (Fig. 1f). Further inspection shows that parameter values in the regime $k_I > k_M$ that produce the negative correlation share a common trait: mature CD27- cells proliferate *and* die faster than immature CD27+ cells. To gain further insight into this behavior we investigated the dependence of $C_{size\text{-}CD27+}$ on the parameter values and stochastic fluctuations analytically and found that larger proliferation and death rates of the CD27- NK cells produce large stochastic fluctuations in the sizes of the CD27- cell populations. Thus, mature CD27- NK cells in a clone could undergo many proliferation events before encountering death, creating larger clones with higher proportion of mature CD27- NK cells. Conversely, the CD27- cells could go through many death events before a proliferation event causing the clone size to shrink (details in Supplementary Text 1).

We investigated whether this model could accurately fit the first (means) and second (variances and covariance) moments of the measured CD27+ and CD27- NK cell populations at 8 days post-infection. We fit the model by minimizing the sum of square errors (SSE) subject to the constraints $C_{size\text{-}CD27+} < -0.2$ and $k_I > k_M$. This parameter configuration cannot accurately

185 capture the moments of the clonal burst data (Fig. 1g). Thus, although the model that
186 incorporates both NK cell proliferation and death is able produce the negative correlation
187 between the clone size and the percentage of CD27+ NK cells in each clone, it poorly describes
188 the distributions of the immature and mature NK cells in the clones.

189 To further investigate the role of NK cell death in explaining the clone size distribution
190 we compared the above two-state models without or with NK cell death based on the theory of
191 model selection using modified Akkaike Information Criterion (AIC_c) (Burnham et al., 2011).
192 We computed the probability distribution function of the number of immature CD27+ (N_I) and
193 mature CD27- (N_M) cells at any time obtained from our stochastic model by solving the
194 corresponding Master equation numerically and computed the Likelihood function for the
195 available clone size distribution data (details in the Materials and Methods section), and then
196 evaluated modified-AIC (AIC_c) for the two models. To keep the computation in a feasible range
197 we used a part (38 out of 56 clone sizes) of the available data where the maximum clone size is ~
198 1000. The subset of clone size data used here also shows a negative value of $C_{size\text{-}CD27+}$. The
199 AICc value for the two-state model with death is over 50 points lower than that for the two state
200 model without death, which clearly show that the data favor the model with NK cell death.
201 Although this approach only models a subset of the data, it also finds that birth and death rates
202 for mature cells are greater than that of immature cells, and that the growth rate of immature cells
203 is greater than that of mature cells. Further details regarding the analysis are provided in the
204 Materials and Methods section and the Supplementary Material. Because of the computational
205 intensive nature of this approach and its agreement with the simpler method of fitting moments
206 with a constraint, we continue with the later approach for subsequent models.
207

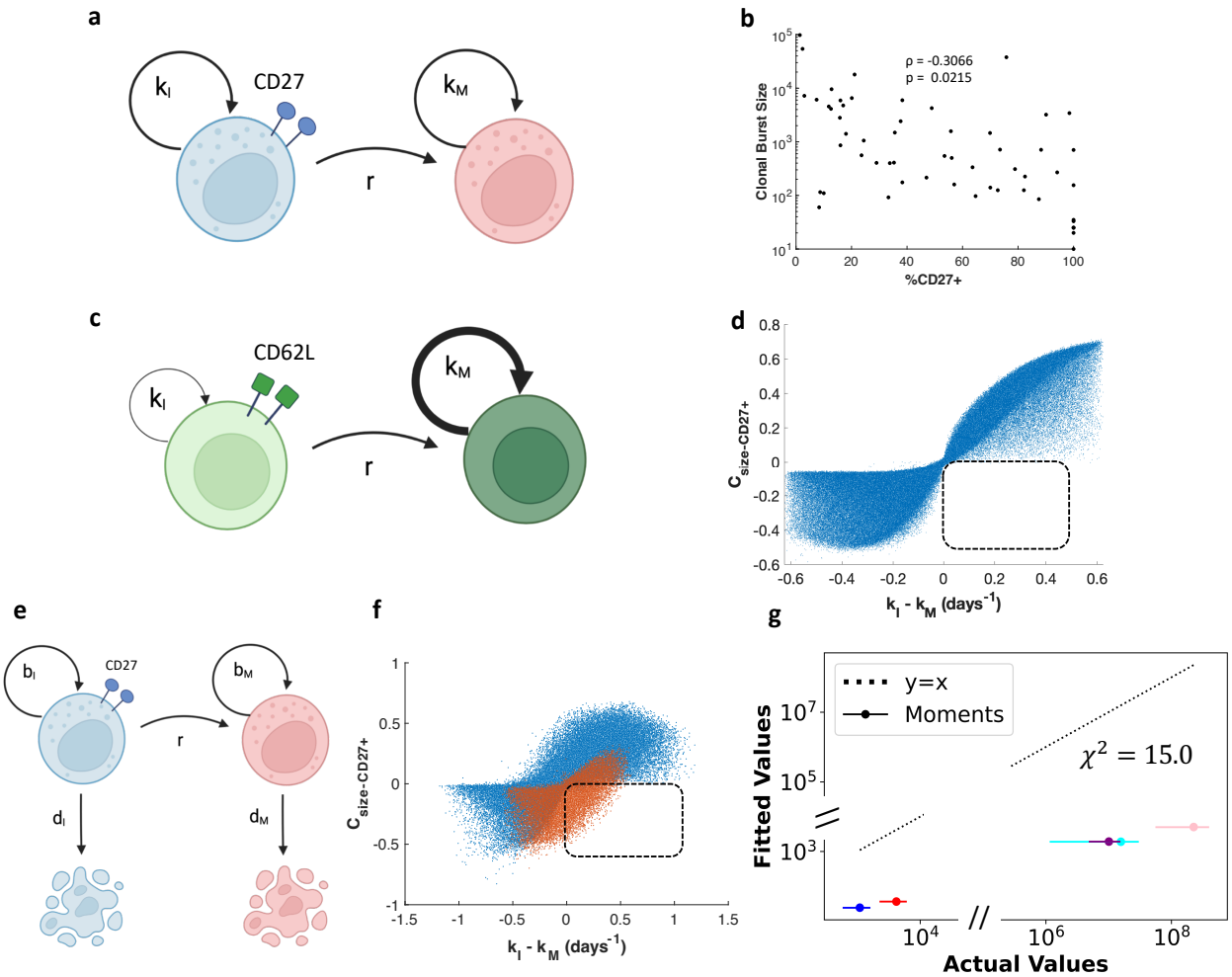

Figure 1: Two-stage linear models cannot capture desired properties of experimental clonal m burst data. (a) Schematic representation of the two-stage model. The model describes immature (CD27+) cells and mature (CD27-) cells. Each cell type has a distinct growth rate (k_I for immature, k_M for mature), and immature cells differentiate to mature cells at rate r. **(b)** Experimental data from Flommersfeld *et al.* display negative value for the correlation $C_{size\text{-}CD27+}$ between clonal burst size and %CD27+ cells. **(c)** Schematic description of antigen specific clonal proliferation and differentiation in CD8+ T cells. Because mature CD62L- cells proliferate more rapidly compared to the immature CD62L+ cells, initial clones made primarily of CD62L- cells

can grow to generate the larger size clones. **(d)** A parameter scan of all possible combinations of k_I, k_M, and r shows that negative correlations ($C_{size\text{-}CD27+} < 0$) are not realized when $k_I > k_M$. Each point represents a value of $C_{size\text{-}CD27+}$ obtained from the model at a unique value of set of model parameters. The parameter configurations that populate the bottom-right quadrant satisfy our two constraints imposed by experimental observations regarding the negative values of $C_{size\text{-}CD27+}$ and higher growth rate of immature NK cells compared to their mature counterparts. **(e)** Schematic representation of the three-state model including cell death. The model has separate parameters for birth of immature (CD27+) cells (b_I), death of immature cells (d_I), birth of mature (CD27-) cells (b_M), death of mature cells (d_M), and differentiation of immature cells to mature (r). In this model, the growth rates are defined as $k_I=b_I-d_I$ and $k_M=b_M-d_M$. **(f)** A parameter scan for this model shows that some parameter configurations can meet the two constraints where $k_I > k_M$ and the parameters result in negative values for $C_{size\text{-}CD27+}$. Each point represents a unique parameter configuration. Red points denote parameter configurations where $b_M > b_I$ <u>and</u> $d_M > d_I$. **(g)** Shows the best fit of the model in (e) to the moments with the constraints $k_I > k_M$ and $C_{size\text{-}CD27+} < -0.2$. Circles represent the fitted values of the first and second moments for the distribution of the NK cell clones obtained from the model. Blue and red circles represent mean populations of CD27+, and CD27- NK cells, respectively. The variances of the CD27+ and CD27- NK cells are shown in cyan and pink circles, and the covariance between the CD27+ and CD27- NK cells is shown in purple. Horizontal lines around the circles show the standard deviations of bootstrapped moments. The solid line is the line $y=x$, which demonstrates where values would lie if we had a perfect fit.

A progressive three-stage differentiation model can quantitatively recreate clonal burst dynamics

We modified our two-state model to include an intermediate state (Fig. 2a) in the model. This reflects many investigations probing NK cell maturation, which show NK cell development goes through several maturation states and some of those states can potentially represent the proposed intermediate state in the model. A well-established NK cell maturation scheme is CD27+CD11b- → CD27+CD11b+ → CD27-CD11b+ (Chiossone et al., 2009). However, the clonal burst data show a negligible proportion of CD11b- NK cells at 8 days post-infection. Another potential maturation scheme could be CD27+KLRG1- → CD27+KLRG1+ → CD27-KLRG1+ (Kamimura and Lanier, 2015). In addition, recent single cell RNA-seq experiments show the presence of CD27-Ly6C+ and CD27-Ly6C- cells at 8 days post-MCMV infection (Riggan et al., 2022), thus the intermediate state could represent a CD27-Ly6C- state as well. Here we present results for the model where the intermediate state represents a mature CD27- state, the other variations of the model are shown in the Supplementary Material (Fig. S3-S5). In order to determine parameter ranges that give rise to higher growth of immature NK cells compared to their immature counterparts, we computed the average size of a clone that originates from either a single CD27+ NK cell or single CD27- NK cell by solving ODEs describing the kinetics of the average NK cell populations. We constructed an effective growth difference metric Δ_k, which describes the difference between the average NK cell populations at day 8 that originate from a single CD27+ or CD27- NK cell at t=0. If Δ_k is positive, then CD27+ cells grow faster than CD27- cells (Materials and Methods). We performed a parameter scan on this three-stage model and find that some parameter configurations with $\Delta_k > 0$ can capture the negative values of $C_{\text{size-}}$

262 $_{CD27+}$ (Fig. 2b). We then evaluated whether this three-stage model can accurately describe the
263 distributions of the immature and mature NK cells in clones. We fitted the means, variances, and
264 the covariance of the NK subpopulations in the clones by varying the model parameters with
265 constraints $\Delta_k > 0$ and $C_{\text{size-CD27+}} < -0.2$ and found that the best-fit three-stage model shows an
266 excellent fit to the data (Fig. 2c, Table 1). Thus, adding an intermediate CD27- stage to the
267 model can capture all the key features of the heterogeneity in the NK cell clonal populations.

268 **Table 1:** Best fit parameters to 3-stage model describing NK clonal bursts given in Fig. 2a.

Parameter	**Estimate (confidence interval)**
b_I	1.064 day^{-1} (1.051 - 1.215)
b_{INT}	1.613 day^{-1} (1.561 - 1.996)
b_M	0.700 day^{-1} (0.001 - 0.727)
d_I	0.054 day^{-1} (0.052 - 0.232)
d_{INT}	0.285 day^{-1} (0.261 - 0.433)
d_M	1.370 day^{-1} (1.330 – 2.000)
r_1	0.126 day^{-1} (0.088 - 0.172)
r_2	0.164 day^{-1} (0.151 - 0.330)

269

270 The three-stage model above makes no assumptions about the identities of the differing
271 phenotypes of the CD27- cell subsets. However, the best fit parameters indicate that the first
272 CD27- subset has a high proliferation rate, and the final CD27- subset has a high death rate.
273 Riggan *et al.* (Riggan et al., 2022) previously determined that, in the contraction phase, Ly6C+
274 NK cells differentiate from Ly6C- cells, and that Ly6C+ cells die more rapidly than Ly6C- cells.
275 Our model shows that similar activity may be observed during the expansion phase as well, as
276 we show higher death of Ly6C+ cells and a unidirectional maturation from Ly6C- → Ly6C+
277 cells. Because our analysis pertains to the expansion phase of the NK cell response to MCMV
278 we thus aimed to validate if the mature states proposed in the model can be identified with
279 CD27-Ly6C- and CD27-Ly6C+ NK cells. We found that our best fit parameters correctly
280 recreate the experimentally observed strong negative correlation between the %CD27+ and
281 %Ly6C+ NK cells across clones (Grassmann et al., 2019), and correctly estimate that most
282 clones have <20% Ly6C+ cells at day 8 post-infection (Fig. 2d-e). This independent validation
283 gives evidence that our parameter estimates can be meaningfully interpreted for a model where
284 NK cells differentiate along a trajectory from CD27+Ly6C- → CD27-Ly6C- → CD27-Ly6C+.
285 We sought to understand the mechanism by which the three-stage model can generate
286 negative values for the correlation $C_{\text{size-CD27+}}$ as well as quantitatively describe the heterogeneity
287 in the NK cell populations in the clones. The two-stage model predictions for the first and the
288 second moments for the NK cell populations are substantially less than the actual values,
289 indicating that our best-fit parameters are not producing enough NK cells (Fig. 1g). The presence
290 of the intermediate state in the three-stage model alleviates this issue, which can rapidly grow
291 and increase the number of CD27-Ly6C+ NK cells while the rapidly dying CD27-Ly6C- NK
292 cells can help meet the constraint that a population of CD27- cells grows slower than one of

CD27+ cells. This variation increases stochastic fluctuations in the observed numbers of CD27- cells, as some clones will have many CD27- cells from high growth of the intermediate Ly6C- subset, while other clones will have few CD27- cells from low growth of the Ly6C+ subset. Furthermore, the presence of the CD27-Ly6C+ NK cells expand the range of the model parameters that can give rise to negative values of $C_{\text{size-CD27+}}$.

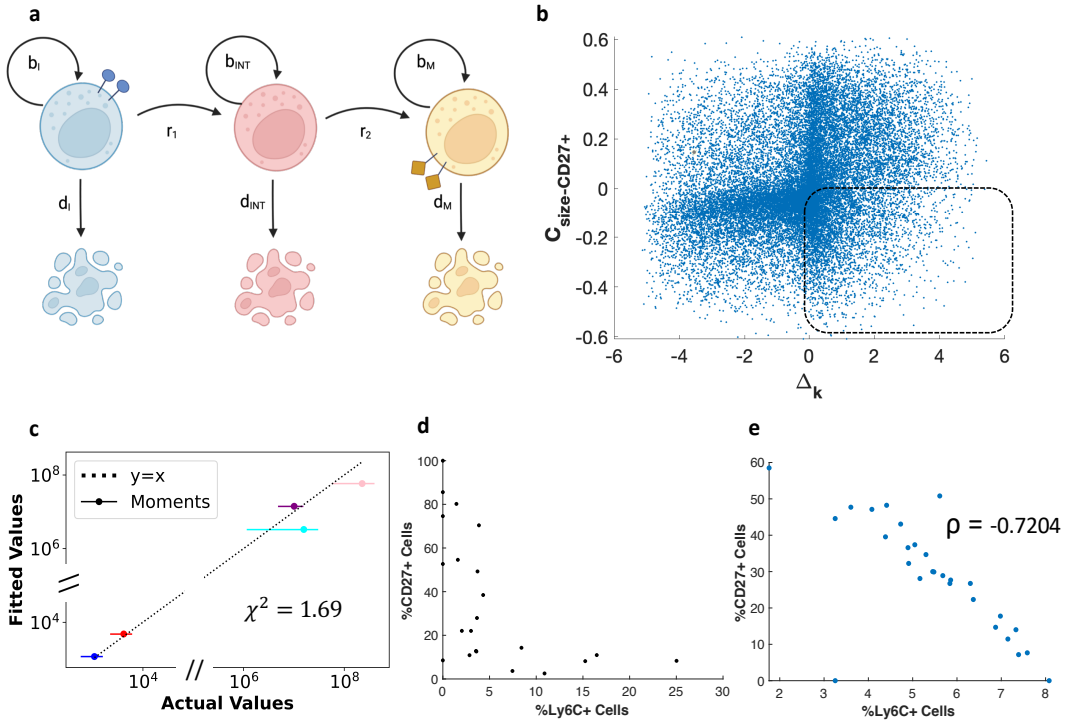

Figure 2: A three-stage linear model can capture experimental observations of NK cell clones if intermediate double-positive NK cells are the fastest growing subset. (a) Schematic representation of the three-stage model. In this model there are three stages of NK cell maturation: an immature (CD27+), intermediate (CD27-), and terminally mature (CD27-) subset. Each subset has a distinct proliferation and death rate, and cells progress from immature to intermediate maturity according to rate r_1 and from intermediate to terminal maturity according to rate r_2. **(b)** A parameter scan for the model in (a) shows that adding a third stage of maturation

306 can account for the negative values in $C_{size\text{-}CD27+}$. Each point represents a unique parameter
307 configuration. Positive values of Δ_k indicate that immature CD27+ cells grow faster than mature
308 CD27- cells and vice versa. See the Materials and Methods for further details. **(c)** Best fit of this
309 model to the moments with the constraints $\Delta_k > 0$ and $C_{size\text{-}CD27+} < -0.2$. Circles represent the
310 fitted values of the moments to the model. Blue and red circles represent mean populations of
311 CD27+, and CD27- NK cells, respectively. The variances of the CD27+ and CD27- NK cells are
312 shown in cyan and pink circles, and the covariance between the CD27+ and CD27- NK cells is
313 shown in purple. Horizontal lines around the circles show the standard deviations of
314 bootstrapped moments. The solid line is the line $y=x$, which demonstrates where values would lie
315 if we had a perfect fit. **(d)** Simulated clones from the three-stage model in (a) at the best fit
316 parameter values shown in (c) when the three stages are taken as immature CD27+Ly6C-,
317 mature CD27-LyC- and the terminally mature CD27-Ly6C+, respectively. Each point is a
318 simulated clone resulting from a single NK cell.
319
320 **Comparison of kinetics between endogenous NK cells, adoptively transferred cells, and**
321 **homeostatic cells identifies potential identical maturation rates in all conditions**
322
323 Here we compare the kinetics of NK cell maturation occurring in response to MCMV infection
324 and in homeostasis. In particular, we investigated the changes in the rates of cell growth and
325 differentiation induced by MCMV infection. First, we quantified the growth and the
326 differentiation rates using time-stamped flow cytometry data on homeostatic NK cells with a
327 one-time treatment of tamoxifen in fluorescent NK cell reporter mice reported by Adams *et*
328 *al*.(Adams et al., 2021). Treating the mice with tamoxifen determines whether observed NK cells

329 are newly populated from bone marrow or existed in peripheral blood at the onset of the
330 infection. We fitted a two-state CD27+ → CD27- maturation model described by ordinary
331 differential equations (see Materials and Methods) to the data collected at days 3, 7, 14, 23, 29,
332 and 35 to estimate the growth rates of the immature CD27+ (k_{CD27+}) and the mature CD27-
333 (k_{CD27-}) NK cells, the rate of differentiation (r) of the CD27+ to CD27- NK cells, and the rate (λ)
334 with which CD27+ NK cells are populated from bone marrow. We estimated these rates both for
335 Ly49H+ and Ly49H- NK cells. The estimated rates for Ly49H+ cells (Table 2, Fig. 3a) show
336 that a CD27+ cell population would double every 6.9 days if there were no differentiation,
337 whereas CD27- cells have a negative growth rate with a half-life of 5.6 days. This implies that
338 the death rate of a population of CD27- cells is greater than their proliferation rate. The
339 differentiation rate from CD27+ → CD27- phenotypes is similar to that of the death rate of
340 Ly49H+ CD27- cells. Approximately 1.37% of the Ly49H+ NK pool is replenished from bone
341 marrow every day. Comparing these rates to those of the Ly49H- NK pool reveals that Ly49H-
342 NK cells are repopulated from bone marrow at almost twice the rate (~2.4%/day). All other
343 estimated rates for Ly49H- NK cells are within the confidence bounds of the Ly49H+ estimated
344 rates (Table 2, Fig. 3b). Given the constraint governing λ which dictates

345 $$\lambda \propto N_{CD27-}$$

346 (Materials and Methods) the difference in estimated λ values can be attributed to a higher
347 percentage of CD27- cells. Next, we compared these rates with corresponding rates estimated in
348 our three-state model using the clonal burst data. The estimate for CD27+ → CD27-
349 differentiation rate is equivalent between Ly49H+ NK cells in homeostasis and in MCMV
350 infection. Our estimations for the clonal burst data (Table 1) show that varying subsets of CD27-
351 cells have varying growth rates ranging -0.7 day^{-1} to 1.3 day^{-1}in MCMV infection, a wide range

352 not in disagreement with the estimate for homeostatic data. Ly49H+ CD27+ cells grow ~10×
353 faster in MCMV infection than in homeostatic conditions.

354 **Table 2:** Best fit parameters to homeostatic Ly49H+ and Ly49H- NK cells.

Parameter	Ly49H+ Estimate (confidence interval)	Ly49H- Estimate (confidence interval)
λ	1.366 percent/day (1.117– 1.594)	2.412 percent/day (2.028 – 2.915)
r	0.125 day^{-1} (0.095 – 0.159)	0.147 day^{-1} (0.118 – 0.173)
k_{CD27+}	0.097 day^{-1} (0.064 – 0.135)	0.088 day^{-1} (0.053 – 0.119)
k_{CD27-}	-0.120 day^{-1} (-0.152 – -0.091)	-0.107 day^{-1} (-0.126 – -0.086)

355

356 We investigated whether the kinetics of NK cell maturation in the expansion phase during
357 MCMV infection in single-cell adoptive transfer experiments is quantitatively similar to that of
358 an endogenous population of NK cells. To this end, we collected time-stamped mass cytometry
359 data on C57BL/6 mice splenocytes at days 0, 4, and 7 post-MCMV infection (Potempa et al.,
360 2022). We then gated Ly49H+ NK cells from each mouse and determined the mean relative
361 abundances across mice of CD27+Ly6C-, CD27-Ly6C-, and CD27-Ly6C+ subsets among the
362 NK cell population (Fig. S6). We multiplied these relative abundances by mean absolute
363 numbers of Ly49H+ endogenous NK cells during MCMV infection from Robbins *et al.*(Robbins
364 et al., 2004) to obtain time-stamped population sizes of NK cell subsets. We then modeled these
365 data with the ordinary differential equation (ODE) solution in Equations S17-S25 using the
366 parameters from Table 1 and an initial condition of the mean uninfected *in vivo* abundances of
367 endogenous NK cells. The ODE result is multiple orders of magnitude above the measured

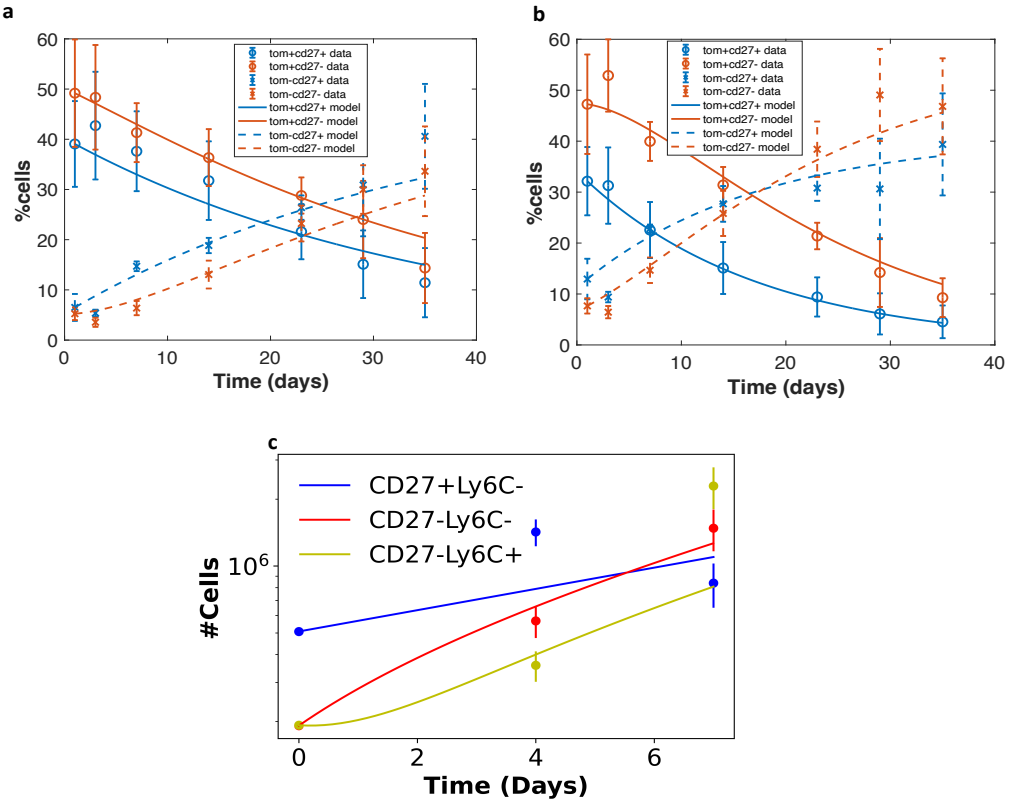

Figure 3: Kinetics of homeostatic NK cells and endogenous NK cells responding to MCMV infection. (a-b) Best fit to **(a)** Ly49H+ and **(b)** Ly49H- homeostatic NK cells. Y axis refers to percentage of the total Ly49H+ or Ly49H- population occupied by that NK subset. Circles and Xs represent the mean values of tamoxifen-induced td-Tomato positive and negative NK cells observed in the data, respectively. Solid and dashed error bars represent standard deviations around the means of tamoxifen-induced positive and negative NK abundances respectively. Smooth curves represent model fits for tamoxifen-induced positive (solid) and negative (dashed) NK cells. (**c**) Best fit to profiled endogenous NK cells responding to MCMV infection. Points represent mean cell abundances, and error bars represent standard deviations of bootstrapped means. Smooth curves represent model fit.

379 abundances (Fig. S7a). This indicates that the kinetics of endogenous NK cells differ
380 significantly from that of NK cells in adoptive transfer experiments.
381 To further quantify the differences in the kinetic rates between the adoptively transferred
382 and endogenous NK cells, we then fit the 3-stage model with 2 mature stages to the endogenous
383 cell population. We used the gated Ly49H+ populations of CD27+/Ly6C-, CD27-/Ly6C-, and
384 CD27-/Ly6C+ NK cells and fit to a system of ODEs that describe the net growth rates of each
385 population and the differentiation rates between them (Materials and Methods). The best fit to
386 this data has unrealistic estimates for the death rate of CD27-/Ly6C+ NK cells and the
387 differentiation rate from CD27+ → CD27- cells (Table S5, Fig. S7b). We then attempted to
388 constrain the fitting procedure by setting the CD27+ → CD27- differentiation rate to those of the
389 previous estimations for the clonal burst kinetics and homeostatic conditions (Tables 1 and 2).
390 Under this constraint, the only rate estimated to be within the confidence interval for the
391 equivalent rate in adoptive transfer experiments is the differentiation rate from Ly6C- → Ly6C+
392 (Table 3, Fig. 3c). The growth rate of CD27+Ly6C- cells is ~4× faster for adoptively transferred
393 cells, the growth rate of CD27-Ly6C- cells is 2-3× faster, and the death rate of mature cells is
394 ~1.5× faster. However, the resulting best fit to the endogenous NK cell population does show
395 that the intermediate CD27-/Ly6C- cell population has the fastest growth rate, and the mature
396 CD27-/Ly6C+ cells have a large death rate, confirming the qualitative results from the adoptive
397 transfer experiments. Thus, although the growth kinetics are different between endogenous and
398 adoptive transfer experiments, both systems have the intermediate population proliferating
399 rapidly and the terminally mature population dying rapidly.
400

401 **Table 3:** Best fit parameters to endogenous NK cells responding to MCMV infection with

402 constrained r_1.

Parameter	Estimate (confidence interval)
k_I	0.236 day^{-1} (0.153 - 0.350)
k_{INT}	0.537 day^{-1} (0.065 - 0.874)
k_M	-0.484 day^{-1} (-1.194 - 0.371)
r_1	0.126 day^{-1} (fixed)
r_2	0.447 day^{-1} (0.000 - 0.874)

403

404 Both the adoptively transferred cells and endogenous population are estimated to have a large
405 death rate for CD27- cells. To test this result, we analyzed NK cell viability in mice that were
406 infected with MCMV at different times post-infection (Fig. 4a). Surprisingly, mature (CD27-)
407 cells indeed had a greater fraction of dead cells than immature (CD27+) cells during expansion
408 (days 4 and 7 post-infection) (Fig. 4b). To determine if the higher rates of cell death in the
409 CD27- NK cell population in the three-state model give rise to a higher fraction of dead NK cells
410 we extended our three-state model to evaluate the number of dead mature and immature NK cells
411 (Fig. S8c) which showed that the best fit parameters for the adoptive transfer experiments are
412 consistent with the results reported above (Fig. 4c). Because we only have best fit growth rates of
413 the endogenous NK cells and not separate proliferation and death rates, we tested a variety of
414 birth and death rates consistent with the best fit parameters such that b-d=k for each cell subset.

415 Many of the possible configurations agree with the higher percentage of live CD27+ cells. This
416 gives additional confirmation that CD27- cells may in fact be dying at faster rates than CD27+
417 cells.

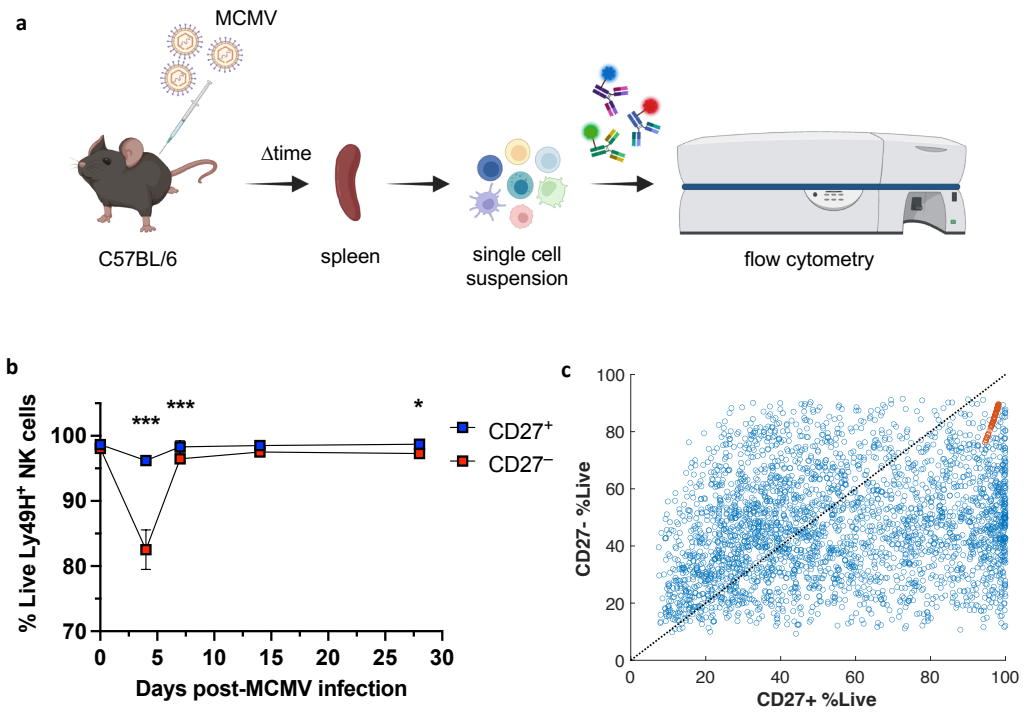

418

419 **Figure 4: Mature CD27- NK cells undergo rapid death during the expansion phase. (a)**
420 Schematic of experimental setup. **(b)** Relative abundances of dead cells for CD27+ (blue) and
421 CD27- (red) *ex vivo* NK cell subsets as measured by flow cytometry experiment. Data are
422 representative of experiments with n = 4-5 mice per timepoint. Graph shows means ± SEM; *P
423 <0.033, and ***P <0.001 represent statistically significant difference between $CD27^+$ and $CD27^-$
424 NK cells as determined by 2-way ANOVA. **(c)** Parameter scans for determining percentage of
425 live cells for CD27+ and CD27- subsets using the model shown in Fig. S8c. Blue points
426 represent a parameter scan where birth and death rates were varied by random sampling such that
427 the growth rates $k_I = b_I - d_I$, $k_{INT} = b_{INT} - d_{INT}$, and $k_M = b_M - d_M$ are equivalent to the kinetic
428 estimates for endogenous NK cells shown in Table 3. Red points represent randomly sampled

429 dead cell clearance rates with other rates set to those describing adoptive transfer kinetics in
430 Table 1. Black dotted line is $y=x$, and points below this line show a higher percentage of live
431 cells for immature CD27+ cells than for mature CD27- cells.

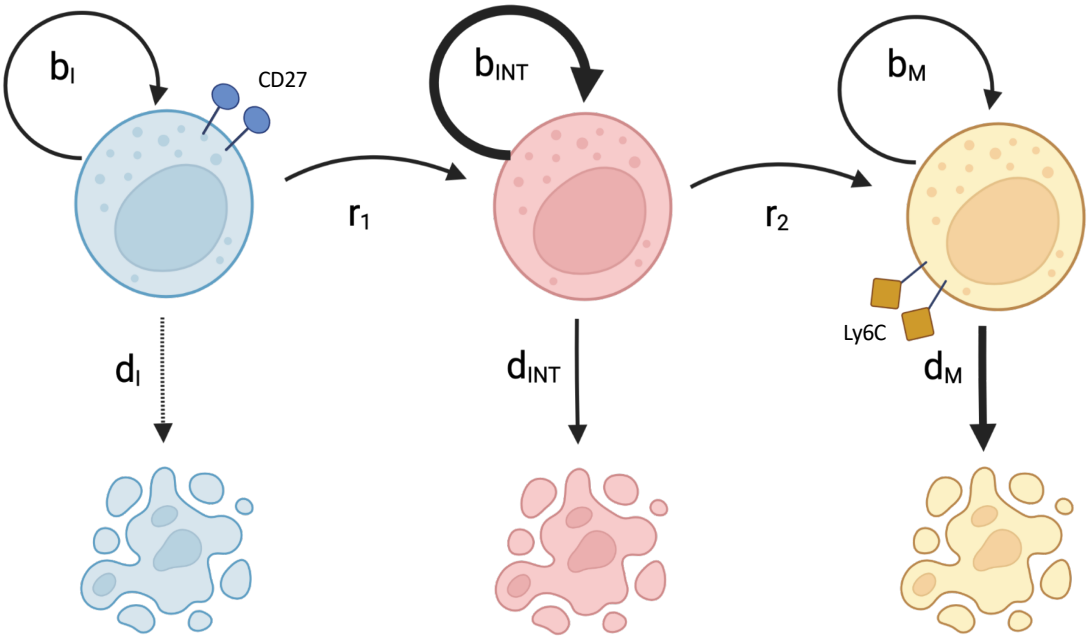

432

433 **Figure 5: Proposed mechanism of NK clonal expansion in response to MCMV infection.**
434 Three distinct subsets of NK cells are necessary to generate full NK response to infection. The
435 first is CD27+, Ly6C-, and moderately proliferative, with a doubling time of ~0.3 days and
436 negligible cell death. The second is CD27-, Ly6C-, and highly proliferative, with a doubling time
437 of ~0.2 days. The last is CD27-, Ly6C-, and prone to rapid cell death with a half-life of ~0.45
438 days. This picture paints CD27-Ly6C- NK cells as having a highly proliferative and highly
439 effective phenotype, similar to effector CD8+ T cells, and CD27+Ly6C- cells as long-lived,
440 similar to memory precursor CD8+ T cells.

441

442 **Discussion**

443

444 We employed stochastic minimal mechanistic *in silico* models to investigate mechanisms that
445 underlie development of MCMV-specific NK cells at early times (0 – 8 days post-infection). We
446 found Ly49H+ NK cells undergoing antigen-specific expansion follow a maturation scheme
447 from (immature) CD27+Ly6C- → (mature I) CD27-Ly6C- → (mature II) CD27-Ly6C+,
448 characterized by a highly proliferative mature CD27-Ly6C- phenotype and a more mature CD27-
449 Ly6C+ phenotype with higher rates of cell death (Fig. 5). The differences in the rates of
450 proliferation and cell death are crucial to give rise to the heterogeneous clones that originate
451 from single immature CD27+ NK cells, in particular, the presence of larger sized NK cell clones
452 composed of mature CD27- NK cells at 8 days post-infection. Similar heterogeneity in the clones
453 of CD8+ T cells generated in the expansion phase (<8 days post-infection) from an acute
454 antigen-specific expansion of single immature CD62L+ cells in C57BL/6 mice has been
455 observed (Buchholz et al., 2013); however, the larger CD8+ T cell clones composed of effector
456 CD62L- arise from the higher rate of proliferation of the CD62L- CD8+ T cells. This is in
457 contrast with the NK cell maturation program where the larger sized clones of mature NK cell
458 populations arise due to the interplay of uneven increase in the proliferation rates and increase in
459 the rates of cell death as the NK cells mature, and intrinsic stochastic fluctuations occurring in
460 these processes. Innate heterogeneity in adoptively transferred single NK cell phenotypes may
461 also contribute to observed stochasticity. In CD8+ T cells, precursor CD62L+ cells are deemed
462 memory precursors, matching their lowly proliferative phenotype (Kretschmer et al., 2020). An
463 equivalent population of memory precursor NK cells has not been identified. CD27-Ly6C+ cells
464 match previously defined phenotypes for memory NK cells and could potentially be memory

465 precursors. However, our model shows that these cells experience rapid cell death. Therefore, for
466 these cells to live longer to become memory cells additional processes such as a change in
467 environmental conditions or an epigenetic change that promotes survival in these cells at later
468 times during the contraction phase could become relevant. This differentiation trajectory is also
469 in contrast with CD8+ T cells, as NK cell memory precursors would be formed downstream of
470 effector (Ly6C-) NK cells, whereas CD8+ effectors (CD62L-) are formed downstream of CD8+
471 T cell memory precursors (CD62L+) in acute infection. Alternately, another mature NK subset
472 such as Ly6C-KLRG1- that is lowly proliferative and long-lived could give rise to the adaptive
473 NK cell phenotype. Inclusion of these processes as well as the later time kinetics could be a
474 future extension of our approach. We note a similarity of our three state NK cell maturation
475 model with maturation of T cells in persistent (13-140 days) *T. gondi* infection in genetically
476 resistant mice reported by Robey and colleagues (Chu et al., 2016) where the infection gave rise
477 to a continuous production of CXCR3-KLRG1+ terminally differentiated effector T cells from a
478 quiescent memory CXCR3+KLRG1- T cells via an intermediate CXCR3+KLRG1+ state. The
479 intermediate T cell state showed higher proliferation and increased death compared to the
480 memory and effector T cells. However, these T cells were uniformly CD62L- in contrast to the
481 memory and effector T cells that are produced in response to acute antigenic SIINFEKL
482 infection.

483 NK cell clones in MCMV infection go through a smaller (~1000×) fold increase in the
484 expansion phase compared that (~40,000×) of antigen-specific expansion of CD8+ T cells. This
485 could be because CD8+ T cells can generate autocrine cytokines such as IL-2 that help the cells
486 to proliferate (Kalia and Sarkar, 2018), whereas NK cells rely on other cells to make the
487 necessary cytokines for proliferation (such as IL-2 and IL-15) and survival (such IL-21) (Fauriat

488 et al., 2010). Furthermore, NK cells are more dependent on cytokines such as IL-15 compared to
489 the CD8+ T cells (DeGottardi et al., 2016). Therefore, cytokine competition for IL-15 and IL-2
490 might also explain increased death of mature NK cells in the expansion phase. A test of this
491 hypothesis could be investigation of MCMV-induced NK cell maturation in *Il15+/-* mice.

492 We quantified the population kinetics of antigen-specific Ly49H+ NK cells during the
493 expansion phase of MCMV infection (<8 days post-infection) using both endogenous and
494 adoptively transferred NK cells. This antigen-specific response was further compared with the
495 kinetics of NK cell maturation in the absence of MCMV infection. Adoptively transferred
496 Ly49H+ NK cells grow at an increased rate compared to the endogenous Ly49H+ NK cells (~3×
497 faster for Ly6C- cells). A possible explanation of this phenomenon is the stronger competition
498 for resources (e.g. antigens and/or cytokines) that would occur in endogenous NK cells could
499 prevent them from growing as quickly as the less dense population of adoptively transferred NK
500 cells. Interestingly, our estimate of the differentiation rate of the immature CD27+ to mature
501 CD27- NK cells showed negligible effect of MCMV infection on this process. This shows that
502 the signaling processes governing NK cell antigen-specific expansion and cytotoxicity are not
503 impacting transcription and translation of CD27, but rather preferential expansion of certain
504 subsets is creating altered phenotype abundances observed in MCMV infection.

505 Our stochastic modeling of heterogeneous NK cell clones showed that larger stochastic
506 variations in the mature NK cell populations arising due to higher intrinsic noise fluctuations
507 generated by the interplay between the higher proliferation and cell death processes are
508 important for producing large clones of mature NK cells at 8 days post-infection. This is in
509 contrast with stochastic kinetics of CD8+ T cells where the larger clones of effector CD62L-
510 CD8+ T cells can arise due to a higher rate of proliferation of these cells even in the absence of

511 any cell death (Buchholz et al., 2013). Our effort to use different models to quantitatively
512 describe the heterogeneity of NK cell clones demonstrate the critical role of the correlation
513 between the clone size and the proportion of the mature NK cells in the clones, $C_{\text{size-CD27+}}$, in
514 screening out mechanisms that are unable to give rise to the observed heterogeneity.
515
516 **Materials and Methods**
517
518 **NK cell development model**
519
520 We modeled the NK cell proliferation, death, and maturation as a continuous time Markov
521 processes where a proliferation or a death event in a NK cell population increases or decreases
522 the population number, respectively, by one cell. A differentiation event changing a NK cell
523 from immature (*I*) to mature (*M*) decreases the NK cell population in state *I* and increases the
524 population in state *M* simultaneously by a single NK cell. The kinetics of the system are given by
525 the Master equation describing the time evolution of the conditional probability for the system to
526 be in a particular state containing different numbers of immature and mature NK cells at any
527 time t given a specific state at $t=0$. The ODEs describing the kinetics of first and second
528 moments can be derived from the Master equation. The solutions are shown in the
529 Supplementary Materials. The first and second moments for the clone size distributions for all
530 our models were calculated by solving the corresponding ODEs.
531
532
533

534 **Stochastic simulations**

535

536 We use the Gillespie algorithm(Gillespie, 1977) for all our stochastic simulations. For two-stage
537 and three-stage models, we initialized the simulation with a single CD27+ NK cell. We evolved
538 the system until 8 days and numbers of CD27+ and CD27- cells in the NK cell clones were
539 recorded. We calculated the correlation $C_{\text{size-CD27+}}$ for the clones by averaging over 10^4 stochastic
540 trajectories.

541

542 **Fitting model to moments**

543

544 The first and second moments $f(\overrightarrow{\theta})$ for the clone size distributions obtained for two- and three-
545 stage models were computed by solving ODEs (Eqs. S2-S6 in Supplementary Text 1 and the
546 ODEs in Supplementary Text 2). The parameter vector $\vec{\theta}$ represents the rates for proliferation,
547 differentiation, and death in the models. To compare the predicted moments $f(\vec{\theta})$ from the
548 model with the actual moments y computed from the data, we used the cost function below:

549 $$\chi^2 = \sum_i \left(\frac{f_i(\vec{\theta}) - y_i}{\sigma_i} \right)^2 + g(\vec{\theta})$$

550 where, σ_i is the standard deviation corresponding to the data used for computing y_i. A penalty
551 function, $g(\vec{\theta})$ is introduced to implement the constrained imposed by sign of the correlation
552 $C_{size\text{-}CD27+}$. We set $g(\vec{\theta})$ to a high value (= 10^4) when $C_{size\text{-}CD27+} > -0.2$ at any value of Δ_k or
553 $C_{size\text{-}CD27+} < 0$ and $\Delta_k < 0$, otherwise $g(\vec{\theta})=0$. This constraint describes the experimental
554 observation that immature CD27- NK cells grow faster than mature CD27+ NK cells in the
555 expansion phase. σ_i is calculated by taking the standard deviation of each moment across 10,000

556 bootstrapped samples of the clones. Minimization of the cost function was performed with the
557 *lmfit* python package, using the 'least_squares' Trust Region Reflective algorithm. Parameter
558 search space was confined from 0.0 to 2.0 day^{-1} for all parameters.
559
560 **Effective Growth Rate for 3-stage system**
561
562 We developed a metric to quantify the difference in the growth rate of immature CD27- and
563 mature CD27+ NK cells for the three-stage model. We computed mean populations of the NK
564 cell subsets at day 8 by solving Eqs. S17-S25 in Supplementary Text 2 for two different initial
565 conditions. In one case we initialized with the immature CD27+Ly6C- cells, and in the other
566 case we initialized with equal proportions of mature CD27-Ly6C- and mature CD27-Ly6C+
567 cells. We then computed the "effective growth difference" (Δ_k) by evaluating the difference in
568 the mean populations of the immature CD27+ and the mature CD27- NK cells at day 8. We
569 performed an asinh(Δ_k) transformation to help visualization of the data in the graphs shown in
570 the manuscript.
571
572 **Parameter scans**
573
574 For parameter scans showing the relationship between growth rates and the correlation between
575 clone size and %CD27+ cells, each parameter is randomly selected from a uniform distribution
576 from 0 to 1.6 day^{-1}. For each parameter set, 10^4 Gillespie simulations were carried out to
577 compute the correlation $C_{\text{size-CD27+}}$ for the NK cell clones at day 8. We performed scans for 10^5
578 different parameter sets.

579 **Ordinary differential equation fits to homeostatic data**

580

581 The growth and differentiation kinetics of populations of CD27+Tom+ (n_1), CD27-Tom+ (n_2),

582 CD27+Tom- (n_3), and CD27-Tom- (n_4) cells in the periphery in homeostasis are given by the

583 ODEs below:

584 $$\frac{dn_1}{dt} = k_{CD27+}n_1 - rn_1$$

585 $$\frac{dn_2}{dt} = k_{CD27-}n_2 + rn_1$$

586 $$\frac{dn_3}{dt} = k_{CD27+}n_3 - rn_3 + \alpha$$

587 $$\frac{dn_4}{dt} = k_{CD27-}n_4 + rn_3$$

588 The CD27+ and CD27- cells grow with rates k_{CD27+} and k_{CD27-} , respectively, and the

589 differentiation CD27+ → CD27- occurs at a rate, *r*. The influx of immature CD27- cells from the

590 bone marrow to the periphery occurs at a rate α. At homeostasis it is reasonable to assume that

591 the sum of all Ly49H+ and the sum of all Ly49H- NK cells were assumed to be constant through

592 time, *i.e.*,

593 $$n_{TOT}(t = 0) = n_{TOT}(t) = \sum_i n_i(t)$$

594 The kinetics of the percentages ($N_i = 100\times(n_i/n_{TOT})$) of each cell type follow the ODEs below:

595 $$\frac{dN_1}{dt} = k_{CD27+}N_1 - rN_1$$

596 $$\frac{dN_2}{dt} = k_{CD27-}N_2 + rN_1$$

597 $$\frac{dN_3}{dt} = k_{CD27+}N_3 - rN_3 + \frac{\alpha}{n_{TOT}}$$

$$\frac{dN_4}{dt} = k_{CD27-}N_4 + rN_3$$

We define $\lambda = \frac{\alpha}{n_{TOT}}$, which describes the influx rate of either the total Ly49H+ or total Ly49H- population as a percentage of the given population. This makes the ODEs which we fit:

$$\frac{dN_1}{dt} = k_{CD27+}N_1 - rN_1$$

$$\frac{dN_2}{dt} = k_{CD27-}N_2 + rN_1$$

$$\frac{dN_3}{dt} = k_{CD27+}N_3 - rN_3 + \lambda$$

$$\frac{dN_4}{dt} = k_{CD27-}N_4 + rN_3$$

We assume the total number of NK cells and the relative abundances of varying subsets do not change with time in homeostasis, therefore,

$$\frac{d(N_1 + N_2 + N_3 + N_4)}{dt} = k_{CD27+}(N_1 + N_3) + k_{CD27-}(N_2 + N_4) + \lambda = 0$$

$$\frac{d(N_1 + N_3)}{dt} = k_{CD27+}(N_1 + N_3) - r(N_1 + N_3) + \lambda = 0$$

$$\frac{d(N_2 + N_4)}{dt} = k_{CD27-}(N_2 + N_4) + r(N_1 + N_3) = 0$$

These constraints lead to equalities between parameters,

$$r = -\frac{k_{CD27-}N_{CD27-}}{N_{CD27+}}$$

$$\lambda = -(k_{CD27-}N_{CD27-} + k_{CD27+}N_{CD27+})$$

615 Thus, by estimating only k_{CD27+} and k_{CD27-}, and using the mean relative abundances of CD27+
616 and CD27- cells across mice and time, we can solve all four rate parameters in the homeostatic
617 state.
618
619 **Ordinary differential equation fits to mass cytometry data**
620
621 We gated Ly49H+ NK cells in the CyTOF studies into three subsets: CD27+Ly6C-, CD27-
622 Ly6C-, and CD27-Ly6C+. Details of the gating are described in the Supplementary Material. We
623 describe the growth and differentiation kinetics of the populations the immature CD27+Ly6C-
624 (N_I), mature CD27-Ly6C- (N_{INT}), and mature CD27-Ly6C+ (N_M) by the ODEs below,

625 $$\frac{dN_I}{dt} = k_I N_I - r_1 N_I$$

626 $$\frac{dN_{INT}}{dt} = k_{INT} N_{INT} + r_1 N_I - r_2 N_{INT}$$

627 $$\frac{dN_M}{dt} = k_M N_M + r_2 N_{INT}$$

628 Where, k_I, k_{INT}, and k_M denote the rates of growth for N_I, N_{INT}, and N_M, respectively. The rates of
629 differentiation for CD27+Ly6C- → CD27-Ly6C- and CD27-Ly6C- → CD27-Ly6C+ are given
630 by r_1 and r_2, respectively. Since the above system of ODEs is autonomous and linear, we can
631 obtain the time dependent solutions analytically and exactly. The analytical solution was
632 numerically evaluated for different values of the rate parameters represented by $\vec{\theta}$. The analytical
633 solutions were evaluated numerically for specific rate constants and initial conditions. We used
634 the estimated population sizes (details in the main text) for the above NK cell subsets in the
635 CyTOF data at t=0 as the initial conditions and computed the population sizes at day 4
636 ($\{N_i(\vec{\theta}$,t=4d)$\}$) and day 7 ($\{N_i(\vec{\theta}$,t=7d)$\}$) by solving the above ODEs for a parameter set $\vec{\theta}$. We

637 then estimated the parameters by $\vec{\theta}$ by fitting the population sizes at day 4($\{y_i(\vec{\theta}$,t=4d)$\}$) and day

638 7 ($\{y_i(\vec{\theta}$,t=7d)$\}$) using the cost function below.

639 $$\chi^2 = \sum_i \left(\frac{N_i(\vec{\theta}, t = 4d) - y_i(t = 4d)}{\sigma_i}\right)^2 + \left(\frac{N_i(\vec{\theta}, t = 7d) - y_i(t = 7d)}{\sigma_i}\right)^2$$

640

641 **Bootstrapping confidence intervals for parameter estimates**

642

643 To assess the confidence intervals for parameter estimates, we randomly sampled the clones with

644 replacement with equal probability, calculated each moment and its standard deviation, and fit

645 the moments as described above. We repeated the process 1,000 times, yielding 1,000 estimates

646 for the parameters θ. We then sorted the parameter estimates by magnitude and took the 2.5th and

647 97.5th percentile for each. These estimates made up the 95% confidence intervals reported here.

648 For estimations of the homeostatic and endogenous NK populations, we sampled a

649 population of mice before sampling errors in measurements for each bootstrap estimate.

650

651 **Animals and MCMV infection**

652

653 C57BL/6 (B6) B6 mice were purchased from the National Cancer Institute at 6 weeks of age and

654 housed in the specific pathogen-free animal facility at the University of California San Francisco

655 (UCSF) in accordance with the guidelines of the Institutional Animal Care and Use Committee.

656 Experiments used mice of both genders, aged 8-12 weeks.

657 B6 mice were infected with 1000 plaque-forming units (PFU) of Smith strain MCMV via
658 intraperitoneal injection. Spleens were acquired different time point following MCMV infection
659 and examined by flow cytometry.
660
661 **Flow Cytometry**
662
663 Splenocytes from uninfected or infected mice were processed into single cell suspensions, RBC
664 lysed, and then stained for flow cytometry. Surface staining was performed using pre-conjugated
665 antibodies in the presence of the viability marker ZombieRed (BioLegend) and were then analyzed
666 on an LSR II cytometer (BD Biosciences). The antibodies used for flow cytometry were: CD3ε
667 (145-2C11), CD19 (6D5), CD49b (DX5), NK1.1 (PK136), KLRG1 (2F1), Ly6C (HK1.4), CD27
668 (LG.3A10), and Ly49H (3D10). All antibodies were purchased from BioLegend, BD Biosciences,
669 or ThermoFisher Scientific. An unconjugated anti-CD16/CD32 antibody (clone 2.4G2, UCSF
670 Antibody Core) was used to block non-specific binding.
671
672 **Mass cytometry**
673
674 Samples were prepared for mass cytometry as previously described (Potempa et al., 2022).
675 Briefly, splenocytes from each mouse were obtained by mechanical dissociation through a 40-
676 μm filter, treated with ACK lysis buffer, and resuspended in PBS + 5 mM EDTA (PBS/EDTA).
677 Cells were stained for viability by mixing 1:1 with PBS/EDTA + 100 mM cisplatin (Enzo Life
678 Sciences) for 1 minute before quenching with PBS/EDTA + 0.5% BSA (Staining Media). One
679 million splenocytes from each mouse was stained with metal-conjugated antibodies against

680 CD16 (Nd144) and CD32 (Eu153) for 15 minutes at room temperature in Staining Media before
681 supplementation with an Fc blocking Ab (clone 2.4G2). After washing in Staining Media, cells
682 were stained with a master mix of 35 additional metal-conjugated antibodies (Table S6) for 30
683 minutes at room temperature. At the conclusion of the staining period, cells were washed in
684 PBS/EDTA before fixation with PBS/EDTA + 3.2% paraformaldehyde and stored at 4º C for 3-5
685 days. One day prior to data acquisition, samples were barcoded using a 20-plex Pd barcoding kit
686 (Fluidigm) per manufacturer protocol, pooled, and fixed again, overnight at 4º C, in a
687 PBS/EDTA + 3.2% paraformaldehyde solution supplemented with a 1:1000 dilution of a
688 191/193 DNA intercalator (Fluidigm). Just prior to acquisition, barcoded samples were pelleted,
689 washed in double-deionized water, and resuspended in double-deionized water with a 1:20
690 dilution of EQ four Element Calibration Beads (Fluidigm). Data were acquired using a CyTOF2-
691 Helios mass cytometer (Fluidigm), which were then normalized and debarcoded prior to
692 analysis.
693
694 **Acknowledgements**
695
696 This work was supported by NIH grant R01AI146581 to J.D. N.M.A. was supported by a
697 Medical Scientist Training Program grant from the National Institute of General Medical
698 Sciences (T32GM007739 to the Weill Cornell/Rockefeller/Sloan Kettering Tri-Institutional MD-
699 PhD Program) and by an F30 Predoctoral Fellowship from the National Institute of Allergy and
700 Infectious Diseases (F30 AI136239). We would like to thank the Ohio Supercomputer Center for
701 computational resources.
702

703 Abel, A.M., Yang, C., Thakar, M.S., and Malarkannan, S. (2018). Natural Killer Cells:
704 Development, Maturation, and Clinical Utilization. Front Immunol *9*, 1869.
705 Adams, N.M., Diaz-Salazar, C., Dang, C., Lanier, L.L., and Sun, J.C. (2021). Cutting Edge:
706 Heterogeneity in Cell Age Contributes to Functional Diversity of NK Cells. J Immunol *206*, 465-
707 470.
708 Adams, N.M., Grassmann, S., and Sun, J.C. (2020). Clonal expansion of innate and adaptive
709 lymphocytes. Nat Rev Immunol *20*, 694-707.
710 Biassoni, R. (2008). Natural killer cell receptors. Adv Exp Med Biol *640*, 35-52.
711 Buchholz, V.R., Flossdorf, M., Hensel, I., Kretschmer, L., Weissbrich, B., Graf, P., Verschoor,
712 A., Schiemann, M., Hofer, T., and Busch, D.H. (2013). Disparate individual fates compose
713 robust CD8+ T cell immunity. Science *340*, 630-635.
714 Burnham, K.P., Anderson, D.R., and Huyvaert, K.P. (2011). AIC model selection and
715 multimodel inference in behavioral ecology: some background, observations, and comparisons.
716 Behavioral ecology and sociobiology *65*, 23-35.
717 Caligiuri, M.A. (2008). Human natural killer cells. Blood *112*, 461-469.
718 Cerwenka, A., and Lanier, L.L. (2016). Natural killer cell memory in infection, inflammation
719 and cancer. Nat Rev Immunol *16*, 112-123.
720 Chiossone, L., Chaix, J., Fuseri, N., Roth, C., Vivier, E., and Walzer, T. (2009). Maturation of
721 mouse NK cells is a 4-stage developmental program. Blood *113*, 5488-5496.
722 Chu, H.H., Chan, S.-W., Gosling, J.P., Blanchard, N., Tsitsiklis, A., Lythe, G., Shastri, N.,
723 Molina-París, C., and Robey, E.A. (2016). Continuous effector CD8+ T cell production in a
724 controlled persistent infection is sustained by a proliferative intermediate population. Immunity
725 *45*, 159-171.
726 DeGottardi, M.Q., Okoye, A.A., Vaidya, M., Talla, A., Konfe, A.L., Reyes, M.D., Clock, J.A.,
727 Duell, D.M., Legasse, A.W., Sabnis, A.*, et al.* (2016). Effect of Anti-IL-15 Administration on T
728 Cell and NK Cell Homeostasis in Rhesus Macaques. J Immunol *197*, 1183-1198.
729 Fauriat, C., Long, E.O., Ljunggren, H.G., and Bryceson, Y.T. (2010). Regulation of human NK-
730 cell cytokine and chemokine production by target cell recognition. Blood *115*, 2167-2176.
731 Flommersfeld, S., Bottcher, J.P., Ersching, J., Flossdorf, M., Meiser, P., Pachmayr, L.O., Leube,
732 J., Hensel, I., Jarosch, S., Zhang, Q.*, et al.* (2021). Fate mapping of single NK cells identifies a
733 type 1 innate lymphoid-like lineage that bridges innate and adaptive recognition of viral
734 infection. Immunity *54*, 2288-2304 e2287.
735 Gillespie, D.T. (1977). Exact Stochastic Simulation of Coupled Chemical Reactions. The Journal
736 of Physical Chemistry *81*, 2340-2361.
737 Grassmann, S., Pachmayr, L.O., Leube, J., Mihatsch, L., Andrae, I., Flommersfeld, S., Oduro, J.,
738 Cicin-Sain, L., Schiemann, M., Flossdorf, M.*, et al.* (2019). Distinct Surface Expression of
739 Activating Receptor Ly49H Drives Differential Expansion of NK Cell Clones upon Murine
740 Cytomegalovirus Infection. Immunity *50*, 1391-1400 e1394.
741 Guma, M., Angulo, A., Vilches, C., Gomez-Lozano, N., Malats, N., and Lopez-Botet, M. (2004).
742 Imprint of human cytomegalovirus infection on the NK cell receptor repertoire. Blood *104*,
743 3664-3671.
744 Hayakawa, Y., and Smyth, M.J. (2006). CD27 dissects mature NK cells into two subsets with
745 distinct responsiveness and migratory capacity. J Immunol *176*, 1517-1524.
746 Hendricks, D.W., Balfour, H.H., Jr., Dunmire, S.K., Schmeling, D.O., Hogquist, K.A., and
747 Lanier, L.L. (2014). Cutting edge: NKG2C(hi)CD57+ NK cells respond specifically to acute
748 infection with cytomegalovirus and not Epstein-Barr virus. J Immunol *192*, 4492-4496.

749 Huntington, N.D., Vosshenrich, C.A., and Di Santo, J.P. (2007). Developmental pathways that
750 generate natural-killer-cell diversity in mice and humans. Nat Rev Immunol *7*, 703-714.
751 Ishiyama, K., Arakawa-Hoyt, J., Aguilar, O.A., Damm, I., Towfighi, P., Sigdel, T., Tamaki, S.,
752 Babdor, J., Spitzer, M.H., Reed, E.F.*, et al.* (2022). Mass cytometry reveals single-cell kinetics
753 of cytotoxic lymphocyte evolution in CMV-infected renal transplant patients. Proc Natl Acad Sci
754 U S A *119*.
755 Kaech, S.M., Wherry, E.J., and Ahmed, R. (2002). Effector and memory T-cell differentiation:
756 implications for vaccine development. Nat Rev Immunol *2*, 251-262.
757 Kalia, V., and Sarkar, S. (2018). Regulation of Effector and Memory CD8 T Cell Differentiation
758 by IL-2-A Balancing Act. Front Immunol *9*, 2987.
759 Kamimura, Y., and Lanier, L.L. (2015). Homeostatic control of memory cell progenitors in the
760 natural killer cell lineage. Cell Rep *10*, 280-291.
761 Kim, K.H., Yu, H.T., Hwang, I., Park, S., Park, S.H., Kim, S., and Shin, E.C. (2019). Phenotypic
762 and Functional Analysis of Human NK Cell Subpopulations According to the Expression of
763 FcepsilonRIgamma and NKG2C. Front Immunol *10*, 2865.
764 Kretschmer, L., Flossdorf, M., Mir, J., Cho, Y.L., Plambeck, M., Treise, I., Toska, A., Heinzel,
765 S., Schiemann, M., Busch, D.H.*, et al.* (2020). Differential expansion of T central memory
766 precursor and effector subsets is regulated by division speed. Nat Commun *11*, 113.
767 Lau, C.M., Adams, N.M., Geary, C.D., Weizman, O.E., Rapp, M., Pritykin, Y., Leslie, C.S., and
768 Sun, J.C. (2018). Epigenetic control of innate and adaptive immune memory. Nat Immunol *19*,
769 963-972.
770 Lopez-Verges, S., Milush, J.M., Schwartz, B.S., Pando, M.J., Jarjoura, J., York, V.A., Houchins,
771 J.P., Miller, S., Kang, S.M., Norris, P.J.*, et al.* (2011). Expansion of a unique CD57(+)NKG2Chi
772 natural killer cell subset during acute human cytomegalovirus infection. Proc Natl Acad Sci U S
773 A *108*, 14725-14732.
774 Martinet, L., Ferrari De Andrade, L., Guillerey, C., Lee, J.S., Liu, J., Souza-Fonseca-Guimaraes,
775 F., Hutchinson, D.S., Kolesnik, T.B., Nicholson, S.E., Huntington, N.D.*, et al.* (2015). DNAM-1
776 expression marks an alternative program of NK cell maturation. Cell Rep *11*, 85-97.
777 Min-Oo, G., Bezman, N.A., Madera, S., Sun, J.C., and Lanier, L.L. (2014). Proapoptotic Bim
778 regulates antigen-specific NK cell contraction and the generation of the memory NK cell pool
779 after cytomegalovirus infection. J Exp Med *211*, 1289-1296.
780 Mitrovic, M., Arapovic, J., Jordan, S., Fodil-Cornu, N., Ebert, S., Vidal, S.M., Krmpotic, A.,
781 Reddehase, M.J., and Jonjic, S. (2012). The NK cell response to mouse cytomegalovirus
782 infection affects the level and kinetics of the early CD8(+) T-cell response. J Virol *86*, 2165-
783 2175.
784 Nabekura, T., Kanaya, M., Shibuya, A., Fu, G., Gascoigne, N.R., and Lanier, L.L. (2014).
785 Costimulatory molecule DNAM-1 is essential for optimal differentiation of memory natural
786 killer cells during mouse cytomegalovirus infection. Immunity *40*, 225-234.
787 Ni, J., Miller, M., Stojanovic, A., Garbi, N., and Cerwenka, A. (2012). Sustained effector
788 function of IL-12/15/18-preactivated NK cells against established tumors. J Exp Med *209*, 2351-
789 2365.
790 Orr, M.T., Sun, J.C., Hesslein, D.G., Arase, H., Phillips, J.H., Takai, T., and Lanier, L.L. (2009).
791 Ly49H signaling through DAP10 is essential for optimal natural killer cell responses to mouse
792 cytomegalovirus infection. J Exp Med *206*, 807-817.

793 Paul, S., Kulkarni, N., Shilpi, and Lal, G. (2016). Intratumoral natural killer cells show reduced
794 effector and cytolytic properties and control the differentiation of effector Th1 cells.
795 Oncoimmunology *5*, e1235106.
796 Peng, H., and Tian, Z. (2017). Natural Killer Cell Memory: Progress and Implications. Front
797 Immunol *8*, 1143.
798 Potempa, M., Aguilar, O.A., Gonzalez-Hinojosa, M.D.R., Tenvooren, I., Marquez, D.M.,
799 Spitzer, M.H., and Lanier, L.L. (2022). Influence of Self-MHC Class I Recognition on the
800 Dynamics of NK Cell Responses to Cytomegalovirus Infection. J Immunol *208*, 1742-1754.
801 Riggan, L., Ma, F., Li, J.H., Fernandez, E., Nathanson, D.A., Pellegrini, M., and O'Sullivan, T.E.
802 (2022). The transcription factor Fli1 restricts the formation of memory precursor NK cells during
803 viral infection. Nat Immunol *23*, 556-567.
804 Robbins, S.H., Tessmer, M.S., Mikayama, T., and Brossay, L. (2004). Expansion and contraction
805 of the NK cell compartment in response to murine cytomegalovirus infection. J Immunol *173*,
806 259-266.
807 Romee, R., Rosario, M., Berrien-Elliott, M.M., Wagner, J.A., Jewell, B.A., Schappe, T., Leong,
808 J.W., Abdel-Latif, S., Schneider, S.E., Willey, S.*, et al.* (2016). Cytokine-induced memory-like
809 natural killer cells exhibit enhanced responses against myeloid leukemia. Sci Transl Med *8*,
810 357ra123.
811 Schlub, T.E., Badovinac, V.P., Sabel, J.T., Harty, J.T., and Davenport, M.P. (2010). Predicting
812 CD62L expression during the CD8+ T-cell response in vivo. Immunol Cell Biol *88*, 157-164.
813 Schlub, T.E., Sun, J.C., Walton, S.M., Robbins, S.H., Pinto, A.K., Munks, M.W., Hill, A.B.,
814 Brossay, L., Oxenius, A., and Davenport, M.P. (2011). Comparing the kinetics of NK cells, CD4,
815 and CD8 T cells in murine cytomegalovirus infection. J Immunol *187*, 1385-1392.
816 Sun, J.C., Beilke, J.N., and Lanier, L.L. (2009). Adaptive immune features of natural killer cells.
817 Nature *457*, 557-561.
818 Vivier, E., Tomasello, E., Baratin, M., Walzer, T., and Ugolini, S. (2008). Functions of natural
819 killer cells. Nat Immunol *9*, 503-510.
820 Voigt, V., Forbes, C.A., Tonkin, J.N., Degli-Esposti, M.A., Smith, H.R., Yokoyama, W.M., and
821 Scalzo, A.A. (2003). Murine cytomegalovirus m157 mutation and variation leads to immune
822 evasion of natural killer cells. Proc Natl Acad Sci U S A *100*, 13483-13488.
823 Yang, S., Liu, F., Wang, Q.J., Rosenberg, S.A., and Morgan, R.A. (2011). The shedding of
824 CD62L (L-selectin) regulates the acquisition of lytic activity in human tumor reactive T
825 lymphocytes. PLoS One *6*, e22560.
826